J Membrane Biol (2011) 242:41–51
DOI 10.1007/s00232-011-9375-5

Comparative Permeabilities of the Paracellular and Transcellular Pathways of Corneal Endothelial Layers

Friedrich P. Diecke · Verónica I. Cacace · Nicolás Montalbetti · Li Ma · Kunyan Kuang · Pavel Iserovich · Jorge Fischbarg

Received: 14 April 2011 / Accepted: 13 June 2011 / Published online: 29 June 2011

Abstract Layers of rabbit corneal endothelial cells were cultured on permeable inserts. We characterized the diffusional permeability of the cell layer to nonelectrolyte and charged molecules and compared the diffusional and filtration permeabilities of the paracellular and transcellular pathways. We determined the rates of diffusion of ^{3}H- and ^{14}C-labeled nonelectrolyte test molecules and estimated the equivalent pore radius of the tight junction. Negatively charged molecules permeate slower than neutral molecules, while positively charged molecules permeate faster. Palmitoyl-DL-carnitine, which opens tight junctions, caused an increase of permeability and equivalent pore radius. Diffusional water permeability was determined with ^{3}H-labeled water; the permeabilities of the tight junction and lateral intercellular space were calculated using tissue geometry and the Renkin equation. The diffusional permeability (P_d) of the paracellular pathway to water is 0.57 μm s^{-1} and that of the transcellular path is 2.52 μm s^{-1}. From the P_d data we calculated the filtration permeabilities (P_f) for the paracellular and transcellular pathways as 41.3 and 30.2 μm s^{-1}, respectively. In conclusion, the movement of hydrophilic molecules through tight junctions corresponds to diffusion through negatively charged pores (r = 2.1 ± 0.35 nm). The paracellular water permeability represents 58% of the filtration permeability of the layer, which points to that route as the site of sizable water transport. In addition, we calculated for NaCl a reflection coefficient of $0.16 \leq \sigma_{NaCl} \leq 0.33$, which militates against osmosis through the junctions and, hence, indirectly supports the electro-osmosis hypothesis.

Keywords Tight junction · Lateral intercellular space · Pore radius · Diffusional permeability · Filtration permeability · Osmotic permeability

Introduction

Leaky epithelial layers, including the corneal endothelium, present two possible routes for transepithelial solute and water transport: (1) the transcellular pathway and (2) the paracellular pathway (lateral intercellular space and tight junction in series). The relative contributions of each of these pathways have not been clearly delineated. It is generally assumed that hydrophobic solutes and solutes for which there are specific active transport mechanisms traverse the endothelial cell layer via the transcellular route. Conversely, hydrophilic solutes are assumed to permeate through the paracellular pathway, with their rate of permeation being determined by the tight junction.

The route for the movement of water remains controversial. According to one school of thought, transcellular solute transport generates local osmotic gradients across the basolateral and apical membranes, which in turn generate transcellular water movement even in epithelia with "leaky" tight junctions (Reuss 2008). However, much evidence has been

Friedrich P. Diecke is now deceased.

F. P. Diecke
Department of Pharmacology and Physiology, UMDNJ-New Jersey Medical School, Newark, NJ, USA

L. Ma · K. Kuang · P. Iserovich
Department of Ophthalmology, Columbia University, New York, NY, USA

V. I. Cacace · N. Montalbetti · J. Fischbarg (✉)
ININCA (Inst. of Cardiological Investigations "A.C. Taquini"), University of Buenos Aires and CONICET, Marcelo T. de Alvear 2270, C1122AAJ Buenos Aires, Argentina
e-mail: fischbargj@fmed.uba.ar

offered for the alternative of paracellular fluid transport (Fischbarg 2010; Shachar-Hill and Hill 2002). In the particular case of the corneal endothelium, the possibility of paracellular electro-osmotic fluid transport was raised years ago (Lyslo et al. 1985), and evidence for it has been advanced in a recent series of publications from our laboratory (Diecke et al. 2007; Fischbarg and Diecke 2005; Rubashkin et al. 2005; Sanchez et al. 2002), as recently reviewed (Fischbarg 2010; Fischbarg et al. 2006). According to these papers, the electrical potential difference across the endothelium generates an electrical current which drives fluid movement by electro-osmotic coupling at the junctions.

The rabbit corneal endothelium and the confluent cultured corneal endothelial cell layers have a translayer electrical specific resistance of 20–30 ohm $\times$ cm^2 (Geroski and Hadley 1992; Lim and Fischbarg 1981; Ma et al. 2007), that is, an electrical conductance of 33–50 mmho cm^{-2}. In contrast, the transcellular conductance of two cell membranes in series is on the order of 0.5 mmho cm^{-2}. Thus, approximately 99% of the electrical conductance of these cell layers resides in the paracellular route. Given such a high electrical conductance, the paracellular pathway can be expected to represent also a pathway for the diffusion of water. We therefore attempted to characterize the permeability of cultured layers of corneal endothelial cells to tritiated water and to hydrophilic solutes ranging from 59 to 640 in MW. As might be expected, permeability values for these solutes are not a simple function of their diffusion coefficient in water but depend instead on their size, suggesting the presence of steric hindrance in the junction. We find that the restricted translayer diffusion of these solutes can be explained by a junctional equivalent pore radius of 2.13 nm. Using solutes of similar molecular weight and size but with different electrical charge sign, we also determined that the pore discriminates and is selective toward positively charged solutes. We also determined the total diffusional permeability to water across the endothelial layer and, by extrapolation, the permeability to water of the paracellular space plus the tight junction in series. The difference between the total water permeability of the cell layer and that of the paracellular space plus junction represents therefore the transcellular permeability to water. We conclude that approximately 18% of the total diffusional water permeability of the cell layers resides in the paracellular route. That percentage rises to 58% for the paracellular filtration water permeability.

Materials and Methods

Cell Culture

Corneas were obtained from New Zealand albino rabbits ($\sim$2 kg) using procedures in accordance with the Guide for the Care of Laboratory Animals (NIH Publication 85–23, revised 1985). Rabbits were killed by injecting a sodium pentobarbital solution into the marginal ear vein, and the eyes were enucleated immediately. The cornea was dissected, placed facedown on a hemispherical support, and a Ca^{2+}–Mg^{2+}-free solution containing 0.25% trypsin and 0.02% EDTA was placed on its concave (endothelial) side for 5–10 min. Then, endothelial cells were dislodged by gentle rubbing in the presence of Dulbecco's modified Eagle medium (DMEM; GIBCO, Grand Island, NY). Cells were aspirated and plated in 25-cm^2 culture flasks (Falcon®; Becton Dickinson, Franklin Lakes, NJ) with 3 ml of DMEM plus 10% heat-inactivated fetal bovine serum, 2 ng ml^{-1} basic fibroblast growth factor and penicillin + streptomycin. Cells were maintained at 37°C in a 5% CO_2 incubator and fed every 3 days. For the experiments, cells were cultured to confluence on Transwell® permeable inserts (Corning Life Sciences, Lowell, MA; polyester membrane product 3450, pore size 0.4 μm, 4 $\times$ 10^6 pores cm^{-2}; polycarbonate membrane product 3412, pore size 0.4 μm, 1 $\times$ 10^8 pores cm^{-2}; membrane thickness for both 10 μm).

Transport Measurements

After complete confluence as determined by microscopic examination and determination of transendothelial resistance (TER) (Ma et al. 2007), the translayer flux of ^{3}H- or ^{14}C-labeled probe molecules was determined using the chamber shown in Fig. 1. The bottom compartment (2 ml, donor compartment), contained physiological buffer solution with 2.5 μCi radiolabeled probe molecules (listed in Table 1). The insert with the cells (receiver compartment) contained 2 ml of physiological buffer solution without labels. The physiological buffer solution contained (in mM l^{-1}) NaCl 113.9, $NaHCO_3$ 26.2, KCl 4.7, NaH_2PO_4 1.0, $CaCl_2$ 1.8, $MgSO_4$ 0.4, D-glucose 5.6, HEPES 10; pH was 7.4 and osmolarity, 290 mOsm.

The assembly was placed on a shaker-bath platform and stirred by horizontal reciprocating motions ($\sim$40 cycles

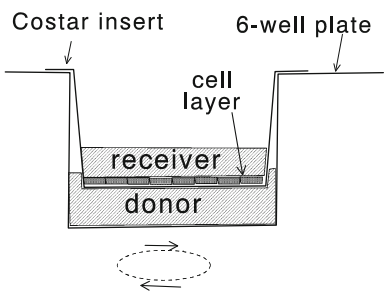

Fig. 1 Chamber for the measurement of radioisotope fluxes. Stirring is indicated

Table 1 Calculated and experimentally determined diffusional permeabilities of Transwell permeable inserts to test solutes

	Insert membrane diffusional permeability (μm s^{-1})			
	Polycarbonate		Polyester	
	Calculated	Experimental	Calculated	Experimental
Urea	8.00	–	0.829	0.920 ± 0.091
Acetamide	7.66	7.98 ± 0.56	0.786	–
Mannitol	4.71	4.80 ± 0.39	0.436	0.490 ± 0.057
Sucrose	3.86	–	0.333	0.360 ± 0.041
Raffinose	3.26	3.44 ± 0.28	0.267	–

To calculate permeabilities, we used the nominal pore density, pore diameter and insert thickness provided by the manufacturer's literature and the free diffusion coefficient of the solute

per minute); temperature was 37°C. At the beginning and the end of the experiment, a 0.1-ml sample of the donor compartment was taken. During the experiments 0.1-ml samples were taken from the receiver compartment at 10-min intervals for the first 30 min and at 30-min intervals for the remaining 2.5 h; each sample volume was replaced with fresh (unlabeled) solution. Samples were mixed with 5 ml of scintillation cocktail and placed in a scintillation counter. Results were plotted as $M_{R(t)}/M_{D(0)}$, where M_R is the radioactivity at time t in the receiver compartment and $M_{D(0)}$ is the radioactivity at time 0 in the donor compartment (Fig. 2). The regular progression of the radioisotope fluxes showed no stirring-induced damage. All experiments were run in quadruplicate.

There are two potential sources of error for these measurements. (1) There is fluid transport from the donor to the receiver compartment (3.96 μl h^{-1} cm^{-2} for cultured bovine corneal endothelia (Narula et al. 1992). Since the area of an insert is 4.52 cm^2, this entails a volume gain of 0.9% per hour for the receiver compartment and an equivalent volume loss for the donor. These minute variations were neglected. (2) The fluid level in the receiver compartment was 0.11 cm higher than that in the donor. It can be calculated that this pressure difference would induce a leak of 0.003 μl h^{-1} cm^{-2} of fluid, for a compartmental volume shift of 0.0006% per hour, which is also negligible.

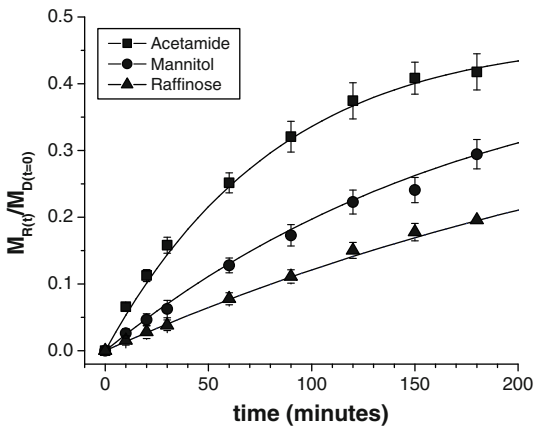

Fig. 2 Rate of appearance of test solute in receiver compartment. The amount of test solute in the receiver compartment at time t ($M_{R(t)}$) is plotted as the fraction of concentration in compartment M_R over the concentration in the donor compartment at time zero ($M_{D(t=0)}$). *Solid lines* represent the fit of Eq. 2 to the data points

Determination of Rate Constant of Exchange and Diffusional Permeability

For experimental arrangements such as the present one, frequently the rate constant (k) for the appearance of radioactivity in the receiver compartment is obtained by fitting the data to an exponential association equation governing the exchange of solute in a closed system of two compartments. However, such a fit would overestimate k since at the end of each interval a 5% fraction of the receiver volume is removed and, with it, label counts. To account for this discontinuous outflow, we devised two different procedures: (1) setting up a difference equation for two compartments, one of them with outflow, and (2) computing the integral of the label counts by averaging the gradient driving the efflux for each period. Both methods give values in close respective agreement.

Method 1, difference equation: $C_{D(t)}$ represents the concentration of label in the donor compartment, $C_{R(t)}$ that in the receiver compartment; k_{12} and k_{21}, the transfer constants for label flows between the donor (1) and receiver (2) compartments. Since the donor and receiver volumes are equal and the area is the same for both flows, $k_{12} = k_{21} = k$, the only parameter thus needed to calculate the permeability of the layer. For completeness, k_{23} is the rate of removal of label from the receiver compartment and Δt is the sampling interval. The difference equations describing the label concentrations in both compartments are

$$C_{D(t)} = C_{D(t-1)} + \left(-C_{D(t-1)} + C_{R(t-1)}\right)k\Delta t \quad (1)$$

$$C_{R(t)} = C_{R(t-1)} + \left(C_{D(t-1)}k - C_{R(t-1)}(k + k_{23})\right)\Delta t \quad (2)$$

$$k = \frac{V_R + V_D}{V_R} \cdot \frac{P_D \cdot A_{ins}}{V_D} = P_D \cdot A_{ins} \quad (3)$$

The rate coefficient, k, is a function of the diffusional permeability (P_D in cm s^{-1}), the area of the permeable insert (A_{ins}) and the volume of the receiver and donor compartments given in Eq. 3, where V_R represents the volume of the receiver compartment and V_D, the volume of the donor compartment.

Junctional Permeability (P_j)

The total diffusional permeability determined (P_D) results from

$$\frac{1}{P_D} = \frac{1}{P_{UL}} + \frac{1}{P_{ins}} + \frac{1}{\left(\frac{P_s P_j}{P_s + P_j} + P_c\right)} + \frac{1}{P_{ULap}} \quad (4)$$

where P_{UL} and P_{ULap} are the permeabilities in series of the unstirred layers on both sides, P_{ins} is that of the plastic insert membrane and P_s and P_J are the series permeabilities of the paracellular space and the tight junction in parallel with the permeability of the cells (P_c).

The permeabilities of the inserts for the different solutes were determined experimentally (Table 1). In addition, the permeabilities of the inserts were computed from the free diffusion coefficient and the pore sizes and densities specified by the manufacturer (Table 1). Unstirred layer permeabilities were obtained as in Beck and Schultz (1970), and the overall permeabilities were corrected on that basis. The permeability values we calculated for a theoretical series arrangement of inserts and unstirred layers were in close agreement with those we determined experimentally. From this, we could assign separate values to P_{UL} and P_{ins}. The importance of these corrections is highlighted in Table 1.

To estimate the equivalent pore radius of the tight junction complexes, the junctional diffusional permeability values obtained were then plotted against the radii of the probe molecules and fit to the Renkin (1954) equation:

$$\frac{A_s}{A_o} = \frac{D_j}{D_f} = \left(1 - \frac{r_s}{r_p}\right)^2 \cdot \left[1 - 2.104 \cdot \left(\frac{r_s}{r_p}\right) + 2.09 \cdot \left(\frac{r_s}{r_p}\right)^3 - 0.95 \cdot \left(\frac{r_s}{r_p}\right)^5\right] \quad (5)$$

In this equation, A_s/A_o represents the fraction of the total pore area available for diffusion of the specific solute, r_s is the radius of the solute molecule and r_p is the equivalent pore radius. Equation 6 contains two unknown variables, r_p and A_s/A_o. We have solved for r_p by replacing A_s/A_o with a proportional term:

$$\frac{P_j}{D_f} = A\frac{A_s}{A_o} \quad (6)$$

P_j represents the permeability of the junction, D_f is the free diffusion coefficient of the solute and the multiplier A is the total pore area per centimeter squared of membrane area divided by the channel length (Rector and Berry 1982). The values for P_j/D_f were plotted against the solute radii (Fig. 3), and r_p was obtained by fitting the Renkin equation to the data points using a nonlinear least square method (Origin 6.1; OriginLab, Northampton, MA).

We also used the Renkin equation for slits (Guo et al. 2003; Preisig and Berry 1985):

$$\frac{A_s}{A_o} = \frac{D_j}{D_f} = \left(1 - \frac{2r_s}{w}\right)^2 \cdot \left[1 - 2.104 \cdot \left(\frac{2r_s}{w}\right) + 2.09 \cdot \left(\frac{2r_s}{w}\right)^3 - 0.95 \cdot \left(\frac{2r_s}{w}\right)^5\right] \quad (7)$$

As above, we substituted into this equation the permeability of the junction as given in Eq. 6.

Estimation of Molecular Radii

The molecular radii of test solutes were calculated from the molecular volumes, assuming spherical geometry. Molecular volumes in turn were calculated as the sum of atomic volumes. The latter were obtained from Lohschmidt (1995) and determined as the ratio of atomic weight and density at the boiling point of the solute.

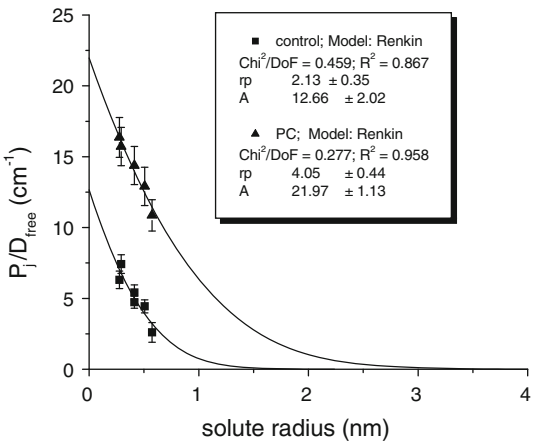

Fig. 3 Extrapolation of equivalent pore radii. Data points represent the ratios P_j/D_f for each test solute plotted against the solute radius in nanometers, both for the control preparations (*filled square*) and for those treated with PC (*filled triangle*). *Curves* represent the nonlinear least squares fits of the Renkin equation (Eqs. 5 and 6) to the data points. Statistics of the fits are also shown

Table 2 Permeability coefficients (in μm s^{-1}) of the cell layer, lateral intercellular space and junction to small nonelectrolyte molecules

Solute	$P_{cell\ layer}$	P_{lis}	$P_{junction}$
Urea	0.62 ± 0.06	1.62	1.05 ± 0.10
Acetamide	0.70 ± 0.06	1.53	1.18 ± 0.13
Mannitol	0.33 ± 0.03	0.84	0.55 ± 0.06
Sucrose	0.29 ± 0.03	0.64	0.44 ± 0.04
Raffinose	0.16 ± 0.01	0.51	0.22 ± 0.02

Statistics

All data points were determined in quadruplicate and are reported as mean ± standard error of the mean (SEM).

Results

Permeability of Permeable Inserts to Hydrophilic Solutes

The initial experiments were conducted on cell layers cultured on polyester inserts. However, it turns out that these inserts have a comparatively low permeability (Table 1), which is of the same order of magnitude as that of the cell layer (Table 2). We therefore changed to polycarbonate inserts, which, according to the manufacturer's specification, have a much higher pore density. Table 1 compares calculated and measured permeabilities of polyester and polycarbonate insert membranes. The permeability of the inserts (P_{ins}) was calculated from the free diffusion coefficients of the solute species and the specifications for pore radius, pore density and insert thickness given by the manufacturer. Table 1 shows good agreement between the calculated and measured permeabilities, but most importantly it also demonstrates that the permeability of polycarbonate membranes is a full order of magnitude greater than that of polyester membranes.

Permeability of Corneal Endothelial Cell Layers to Hydrophilic Solutes

Figure 2 shows an example of measurements of solute flux from the donor compartment to the receiver compartment. The curves represent the nonlinear least squares fits to the data points using Eqs. 2 and 3. These equations provide a value for the rate constant for the solute exchange between the donor and receiver compartments. From this rate constant we calculated the permeability coefficient (P_D) of the complex consisting of permeable insert, unstirred layers and cell layer using Eq. 4 and then obtained the permeability coefficient for the tight junction using Eq. 4. The values for permeability constants for the cell layer, lateral intercellular space and junction are listed in Table 2.

The values for permeability of the junction show a striking decrease with increasing solute size, suggesting a "hindrance" of diffusion in the pore-like structure of the junction. This "hindrance" of diffusion can be used to estimate the equivalent radius of the pores using Eq. 6 proposed by Renkin (1954). This equation correlates the ratio of D_f/D_f (diffusivity in the junction/diffusivity in free solution) to a function of the ratio of solute radius to pore radius. Since we do not know the diffusivity of solutes in the pores of the junction, we substituted the ratio of permeability of the junction and free diffusion coefficient (P_f/D_f), which is proportional to the term D_f/D_f (Rector and Berry 1982).

Figure 3 shows a least squares fit of the Renkin equation to the ratios P_f/D_f of the test molecules. The best fit is obtained assuming an equivalent pore radius of 2.13 ± 0.35 nm. Similarly, using the Renkin equation for slits (Eq. 7), the best fit is for a half-slit width of 2.22 ± 0.36 nm (data not shown). The goodness-of-fit statistics are similar for both cases.

There is some uncertainty about the molecular radii of solutes, and slightly different values for this parameter are obtained depending on the method of determination. In Table 3 we compare two sets of different molecular radii used by Beck and Schultz (1970) and Renkin (1954) with the values used in our work. Beck and Schultz obtained molecular radii from the Stokes-Einstein equation and a correction algorithm to values obtained with that equation proposed for small molecules by Gierer and Wirtz (1953). Renkin estimated molecular radii three different ways: (1) assuming the molecule to approximate a sphere with a volume given by the molecular weight and the density of the substance, (2) from the Stokes-Einstein equation and (3) from the Stokes-Einstein equation and the correction proposed by Gierer and Wirtz (1953). For each molecule species, he then averaged the two closest values and used that value in the estimation of pore radius. In the last row of Table 3 we have listed the pore radii calculated with the different sets. Using the solute radii of Renkin (1954) predicts a pore radius of 2.05 ± 0.21 nm, while calculations based on the radii of Beck and Schultz (1970) yield a

Table 3 Molecular radii (in nm) of test solutes used by different investigators: bottom row lists the equivalent pore radii computed using the respective solute radii values

Solute	Renkin (1954)	Beck and Schultz (1970)	This study
Urea	0.27	0.264	0.286
Acetamide	–	–	0.301
Glucose	0.357	0.444	–
Mannitol	–	–	0.422
Sucrose	0.44	0.555	0.512
Raffinose	0.56	0.654	0.582
Pore radius (nm)	2.05 ± 0.21	2.94 ± 0.64	2.13 ± 0.35

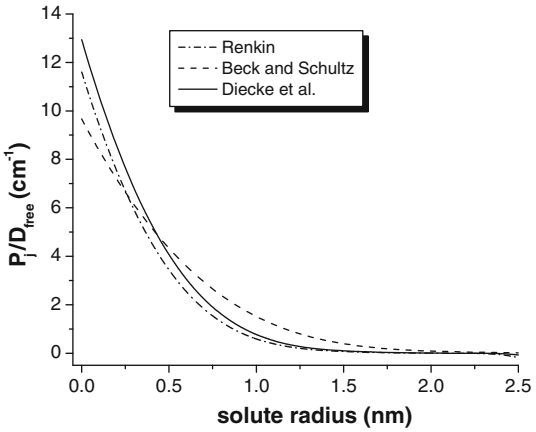

Fig. 4 Comparison of fits of Renkin equation to permeability data using solute radii proposed by different investigators

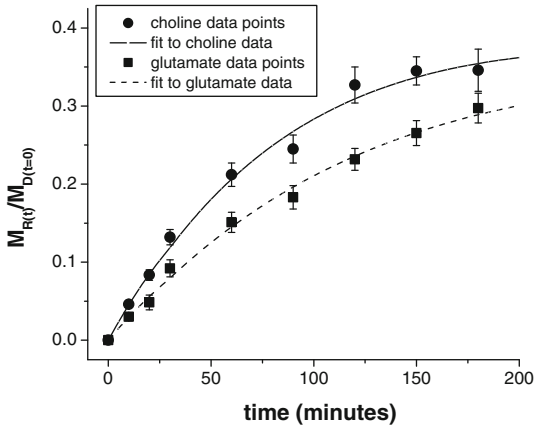

Fig. 5 Comparison of the rate of appearance of a cationic solute, choline, in the receiver compartment to that of an anionic solute, glutamic acid. *Curves* represent the nonlinear least squares fit of Eq. 2 to the data points

pore radius of 2.94 ± 0.64 nm. A visual comparison of the fits is given in Fig. 4.

Effect of Charge on Junctional Permeability

In addition to size selectivity, tight junctions possess charge selectivity (Van Itallie and Anderson 2006). We tested this property by comparing the permeability of choline and glutamic acid. Although these molecules have very similar radii of 0.397 and 0.392 nm, respectively, their rates of diffusion from donor to receiver compartment differ by approximately a factor of 2 (Fig. 5). Figure 6 compares the P_j/D_f ratio for choline and glutamic acid with the P_j/D_f ratio of neutral solutes. The cationic solute shows less restriction of diffusion than neutral solutes of similar size, while the anion has a lower P_j/D_f ratio than neutral solutes.

Effect of PC on Paracellular Permeability

Palmitoyl-DL-carnitine (PC) has been shown to greatly increase the permeability of confluent cultured $CACO_2$ cell layers to small nonelectrolyte and ionic solutes (Knipp et al. 1997) and to decrease in a dose-dependent manner the TER of cultured corneal endothelial cell layers (Ma et al. 2007). We examined the effect of PC on the permeability of confluent layers of cultured corneal endothelial cells to test molecules. Cell layers were pretreated with 0.2 mM PC for 90 min, and then the rate of diffusion of small nonelectrolytes was measured as described in Materials

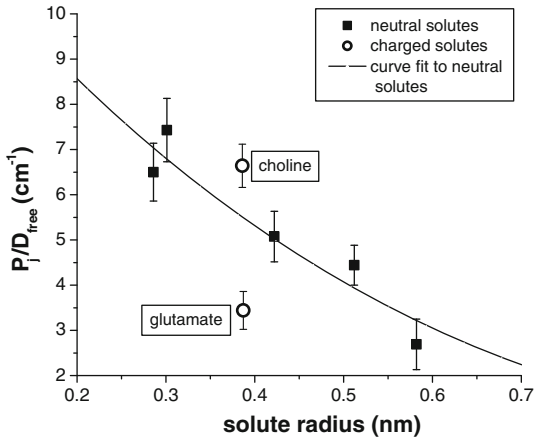

Fig. 6 Modified rates of diffusion for a cationic (choline) and an anionic (glutamate) solute compared with neutral solutes. The P_j/D_f ratio for solutes is plotted against the solute radius. *Curve* represents the fit of the Renkin equation to the data points for neutral solutes

and Methods. Figure 7 compares the rates of appearance of acetamide in the receiver compartment after pretreatment with PC with the control (see Fig. 2) and demonstrates a highly significant increase in permeability due to PC pretreatment. Conversely, it also indicates that no significant stirring damage took place in untreated preparations, which preserved their steric and electrical charge filtering abilities throughout. In Fig. 3 we have plotted the P_f/D_f ratios and estimated the equivalent pore radius after PC treatment as 4.05 ± 0.44 nm, approximately twice as large as that in physiological solutions.

Diffusional Permeability of Cell Layer and Paracellular Pathway to Tritiated Water

The permeability of corneal endothelial cell layers to tritiated water (^3H_2O) was determined using the same protocol as used for the measurement of the permeability of hydrophilic solutes. As shown in Fig. 8, tritiated water

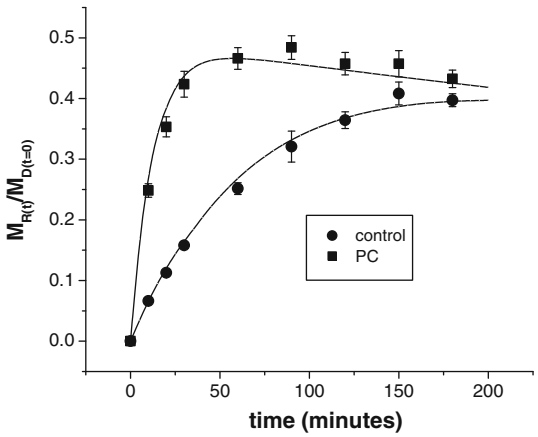

Fig. 7 Diffusion of acetamide from the donor compartment to the receiver compartment before and after exposure to 0.2 mM PC

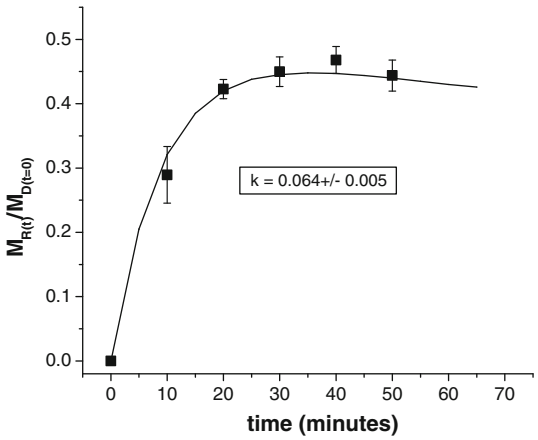

Fig. 8 Rate of appearance of ^3H_2O in the receiver compartment; the value of k comes from the fit of Eq. 2

permeates rapidly from the donor compartment to the receiver compartment; the calculated permeability coefficient is 2.36 μm s^{-1}. After correction for the resistance of the permeable insert and unstirred layers, we obtained a diffusional permeability coefficient of 3.09 μm s^{-1} for the cell layer. This value represents the permeability of the cellular pathway (P_c) in parallel with the permeability of the paracellular pathway, consisting of tight junction (P_j) and lateral intercellular space (P_{lis}).

Discussion

The objectives of our investigation were (1) to characterize the permeability of the tight junction and lateral intercellular space of corneal endothelial cell layers to nonelectrolyte molecules and charged solutes and (2) to determine the diffusional and filtration permeability of the paracellular and transcellular pathways to water.

Permeability of Tight Junction and Lateral Intercellular Space to Small Molecules

The tight junction has been modeled as a barrier system penetrated by size- and charge-selective pores that vary in size from 0.4 to 4 nm and control the flow of solutes and solvent through the barrier (Van Itallie and Anderson 2004, 2006). Our results are consistent with this model. As shown in Table 2, the permeability of small nonelectrolyte molecules decreases as a function of molecular weight and volume. A fit of the Renkin equation to these values predicts an equivalent pore radius of 2.13 nm. This value is in close agreement with the value of 3.9 nm for the junctional width calculated from the steady-state values of hydraulic coefficient (L_p) and cell perimeter/unit area by Fischbarg et al. (1977). Reports of the permeation of large dextran fractions (~70 kDa) through corneal endothelium (Kim et al. 1971) can be explained by the fact that large dextran molecules can snake their way through narrow pores. Of course, numerical conclusions may be limited by the present choice of the Renkin model, which does not take into account shape and tortuosity factors. But the choice of model does not invalidate the finding that steric and electrical charge filters exist and dictate junctional properties.

Charge Selectivity of the Tight Junction

Our results also confirm the charge selectivity of the tight junction pores of corneal endothelial layers. Choline and glutamate have nearly identical molecular radii of 0.397 and 0.392 nm, respectively; however, the rate of diffusion of choline from the donor to the receiver compartment is approximately twice as fast as that of glutamate (Fig. 5). A

comparison of the P_j/D_f ratio (Fig. 6) shows that the effective pore area for glutamate is significantly smaller than that for neutral molecules of equal radius, while the effective pore area for choline is larger. The pores of tight junctions of corneal endothelial cell layers thus have an approximate 2:1 selectivity for positively charged solutes over negatively charged ones. These results are in agreement with the selectivity ratio for Na^+/Cl^- of 2 calculated by Fischbarg and Diecke (2005) and with selectivity data reported by Lim et al. (1983).

Reflection Coefficient σ

Knowledge of the equivalent pore radius permits us to estimate another important parameter, the reflection coefficient σ. The reflection coefficient of a solute is a function of the effective filtration areas of a pore for the solute and water and can be expressed by the following equation (Durbin 1960):

$$1 - \sigma = \frac{A_{sf}}{A_{wf}} \tag{8}$$

where A_{sf} stands for the effective pore area of the solute and A_{wf} is the effective filtration area for water. A_{sf}/A_{wf} represents the ratio of the filtration equation for the solute over that for water (Renkin 1954):

$$\frac{A_{sf}}{A_{wf}} = \frac{\left[2\left(1-\frac{r_s}{r_p}\right)^2 - \left(1-\frac{r_s}{r_p}\right)^4\right]\left[1 - 2.104\left(\frac{r_s}{r_p}\right) + 2.09\left(\frac{r_s}{r_p}\right)^3 - 0.95\left(\frac{r_s}{r_p}\right)^5\right]}{\left[2\left(1-\frac{r_w}{r_p}\right)^2 - \left(1-\frac{r_w}{r_p}\right)^4\right]\left[1 - 2.104\left(\frac{r_w}{r_p}\right) + 2.09\left(\frac{r_w}{r_p}\right)^3 - 0.95\left(\frac{r_w}{r_p}\right)^5\right]} \tag{9}$$

For an equivalent pore radius of 2.13 nm, this equation predicts values for σ of 0.156 for acetamide, 0.331 for mannitol, 0.451 for sucrose and 0.536 for raffinose. These values are lower than those of 0.6 and 0.9 reported for urea and sucrose, respectively, by Mishima and Hedbys (1967). The latter values would be consistent only with pore radii on the order of 0.6 nm, much narrower than presently reported. Our data also permit us to estimate an approximate value for the reflection coefficient of NaCl, the major solute in physiological solutions. Fischbarg and Diecke (2005) calculated permeability coefficients for Na^+ and Cl^- of 6.5×10^{-5} and 3.2×10^{-5} cm s^{-1}, respectively. The value of the permeability coefficient for Na^+ is slightly less than that for acetamide, while the permeability of Cl^- is slightly greater than that of mannitol (Table 2); it is therefore reasonable to assume that the reflection coefficient for NaCl is between that of acetamide (0.156) and mannitol (0.331). Hodson and Lawton (1987) reported a reflection coefficient for NaCl of 1 for the corneal endothelium of rabbit. However, their value is based on the assumption that the endothelial water permeability is much greater than that of the stroma. Other investigators have reported reflection coefficients for NaCl closer to our range: 0.4 (Green and Green 1969), 0.43–0.63 (Klyce and Russell 1979) and 0.6 (Mishima and Hedbys 1967). The range we calculate for σ_{NaCl} (0.16–0.33) militates against the possibility of sizable osmotic fluxes across the junctions.

Diffusional and Filtration Permeability of Paracellular and Transcellular Pathways to Water

Permeability of Cultured Corneal Endothelial Layers to Tritiated Water (^3H_2O): Diffusional Permeability

The combined permeability of the unstirred layer plus insert plus the cells is 2.36 μm s^{-1}. The permeability of the insert is 14.2 μm s^{-1}. The "permeability" of the unstirred layer δ is: $P_{ul} = D_w/\delta = 33.7$ μm s^{-1}, where $\delta = 91$ μm, and D_w is the self-diffusion coefficient of water at 37°C, $D_w = 3.063 \times 10^{-5}$ cm^2 s^{-1}. Correcting for these leads to a value for the cell layer of $P_{layer} = 3.09 \pm 0.16$ μm s^{-1}. Note the error of ~5%.

This value for P_{layer} is in good agreement with results obtained for the corneal endothelium of in vitro corneal preparations. Mishima and Trenberth (1968) measured a P_{layer} of 1.64 μm s^{-1}; Donn et al. (1963) determined the rate of diffusion from stromal to aqueous side in depithelialized cornea and, after correction for diffusion resistance of the stroma, arrived at a P_{layer} value of 2.42 μm s^{-1}.

We subsequently calculated the diffusional permeabilities of the transcellular and paracellular pathways:

$$P_{layer} = \left(\frac{P_{lis} \cdot P_j}{P_{lis} + P_j}\right) + P_{cell} \tag{10}$$

Here, P_j represents the permeability of the junction and P_{lis} is the permeability of the lateral intercellular space. The term in parentheses represents the permeability coefficient of the paracellular pathway (P_{para}).

The values we used for the junctions are equivalent pore radius $r = 21.5$ Å, cell perimeter $p = 1019$ cm cm^{-2} and junction length $lj = 1$ μm:

$$Pj = \frac{\pi \cdot D_w \cdot p \cdot r}{2 \cdot lj} = 1.05\,\mu\text{m s}^{-1} \quad (11)$$

P_{lis} can be calculated from the geometry of the lateral intercellular space. We use a larger perimeter since the intercellular spaces are "skirt-like" (Hirsch et al. 1976):

$$ps = \frac{p + 3.8 \cdot p}{2} = 2446\,\text{cm cm}^{-2} \quad (12)$$

The other values are the width $ws = 200$ Å and the length of the spaces $ls = 12$ μm. The permeability of the lateral intercellular spaces is

$$Ps = \frac{Dw \cdot ps \cdot ws}{ls} = 1.25\,\mu\text{m s}^{-1} \quad (13)$$

Using Eq. 10 above, we calculate for the permeability of the paracellular pathway

$$P_{para} = 0.57\,\mu\text{m s}^{-1}$$

and for the permeability of the transcellular pathway

$$P_{cell} = 2.52\,\mu\text{m s}^{-1}$$

So far, 18% of the diffusional permeability of the layer resides in the paracellular pathway and 82% in the transcellular pathway.

Permeability of Cultured Corneal Endothelial Layers to Tritiated Water (^3H_2O): Osmotic Permeability

Symbols are similar, except for the addition of an "f" (for filtration).

The vast majority of epithelia exhibit comparatively higher permeability values if the flow of water is induced by osmotic or hydrostatic gradients rather than by a diffusional gradient of ^3H_2O. As explanation it has been argued that the bulk flow of water through large cylindrical pores or slits, as represented by the tight junction, would be laminar following Poisseuille's law, while the diffusion of water would be governed by Fick's first law of diffusion. The relationship of osmotic permeability (P_f) to diffusional permeability (P_d) thus can be expressed by the ratio of Poisseuille's law for laminar flow over Fick's first law of diffusion (Thau et al. 1966).

$$\frac{P_f}{P_d} = 1 + \frac{R \cdot T}{8 \cdot \eta \cdot D_w \cdot V_w} \cdot r^2 \text{ for pores} \quad (14)$$

$$\frac{P_f}{P_d} = 1 + \frac{R \cdot T}{3 \cdot \eta \cdot D_w \cdot V_w} \cdot r^2 \text{ for slits} \quad (15)$$

where R is the universal gas constant, T is the absolute temperature, η is the viscosity of water, V_w is the partial molar volume of water and r is equivalent pore radius. For dilute solutions (Schafer and Andreoli 1986), the above equations can be rewritten as

$$P_f = P_d \cdot \left(1 + 0.08 \cdot r^2\right) \text{ for pores or } P_f = P_d \cdot \left(1 + 0.213 \cdot r^2\right) \text{ for slits}$$

where r (pore radius, or slit half-width) is in Ångstrom units.

Osmotic Permeability of the Junction

We use the P_f/P_d ratio above for pores of radius 21.5 Å. We obtain $P_{fj} = 41.7$ μm s^{-1}.

Osmotic Permeability of the Lateral Intercellular Spaces

We use the P_f/P_d ratio for slits 200 Å wide. The corresponding P_{flis} is 4.34×10^3 μm s^{-1}.

Osmotic Permeability of Aquaporin Channels

Water molecules traverse aquaporin channels in single file. The number of water molecules (n_w) that can occupy the channel at any given time is 12 (Zhu et al. 2004). The osmotic permeability of aquaporin channels is given by (Lea 1963):

$$P_{fc} = P_c \cdot n_w = 30.2\,\mu\text{m s}^{-1}$$

Finally, we calculate the osmotic permeability of the paracellular pathway as $P_{fpara} = 41.31$ μm s^{-1}.

The osmotic permeability of the layer is $P_{fl} = 68.4$ μm s^{-1}. The relative contributions to it are 58% by the paracellular pathway and 42% by the transcellular pathway.

Table 4 summarizes these calculations, and Fig. 9 clarifies the geometry involved.

The value for transendothelial permeability is in close agreement with that reported for the in vitro rabbit cornea (Fischbarg et al. 1977). It is, however, significantly lower than values calculated from the swelling or imbibition pressure of the corneal stroma. Swelling pressures ranging

Table 4 Summary of the calculated diffusional and filtration water permeability coefficients for the cell layer and its components

	Diffusional permeability (P_d, μm s^{-1})	Filtration permeability (P_f, μm s^{-1})
P_{layer}	3.09	71.5
P_{cell}	2.52	30.2
$P_{paracellular}$	0.57	41.3
P_j	1.05	41.7
P_{lis}	1.25	4.3×10^3

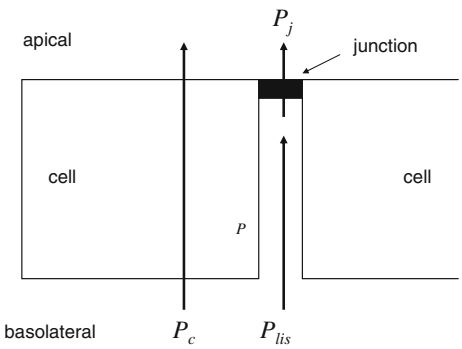

$$P_{layer} = P_c + \frac{P_{lis} \times P_j}{P_{lis} + P_j}$$

Fig. 9 Scheme of water diffusion across cultured rabbit corneal endothelial cells

from 42 mm Hg (Hodson et al. 1991) to 84 mm Hg (Olsen and Sperling 1987) have been measured, with several authors reporting values of 60 mm Hg. Assuming a mean fluid movement of 40–50 cm h^{-1}, this corresponds to a hydraulic coefficient (*Lp*) ranging from 1.8 to 2.3×10^{-8} cm s^{-1} mm Hg^{-1} or a filtration permeability (P_f) of 2.0–2.5 cm s^{-1}. These values are approximately twice as high as the values reported in this study. There is a possibility that our method underestimates the permeability of cultured cell layers. Only a fraction of the area of the lateral intercellular space and of the basal membrane is in direct apposition to the pores of the permeable insert. Thus, there is an additional resistance to diffusion and convection interposed between the porous insert and the lateral intercellular space and basolateral membrane, possibly leading to an underestimate of the permeability of the cell layer and its components (Table 4).

The transcellular filtration permeability is 21×10^{-4} cm s^{-1}. Assuming approximately equal permeability of the apical and basolateral membranes, the cell membrane permeability would be 42×10^{-4} cm s^{-1}. This value is of the same order of magnitude but by a factor of 2 lower than that reported by Echevarria et al. (1993) for plated corneal endothelial cells (93×10^{-4} cm s^{-1}). Again, a possible reason for the difference may be the underestimation of the permeability of the lateral intercellular space and basolateral membrane discussed above.

A significantly higher permeability of the apical cell membrane of corneal endothelial cells has been reported by Sun et al. (2001). Permeability was calculated from the rate of volume change of confluent cultured cells exposed to hyperosmolar solutions at the apical side. Assuming that all transmembrane water flux occurred through the apical membrane only, the authors calculate a filtration permeability of 460×10^{-4} cm s^{-1}. However, if one considers the relatively high permeability of the junctional complex, fluid movement may not have been restricted to the apical membrane but may have also taken place across the lateral membrane, which may have led to an overestimate of the apical cell membrane permeability.

The endothelial fluid transport system has a characteristic: As cells are lost from the endothelial population, it retains its transport characteristics until a threshold cell density is reached ($\sim$500 cells mm^{-2}), at which point transport fails (Sobottka Ventura et al. 2001). The electro-osmosis hypothesis can account for this finding; as the cell density decreases, so does the junctional perimeter; and the junctional resistance increases. The local current increases as long as the electromotive force of the pump can take the added load; however, this compensation has a limit, and when the cell density threshold is reached, it eventually fails.

Our results establish that the paracellular pathway has a higher filtration permeability to water than the transcellular pathway and thus should represent a main route of fluid movement across the corneal endothelium. This conclusion is consistent with those of recent reports in which we have provided experimental evidence (Diecke et al. 2007; Sanchez et al. 2002) and model calculations (Fischbarg and Diecke 2005; Rubashkin et al. 2005), which suggests electro-osmotic coupling of fluid and Na^+ current in the tight junction.

Acknowledgements This work was supported by NIH grant EY06178 and by CONICET grant PIP 01688, both to J. F., who is a career investigator with the Argentine National Research Council (CONICET).

References

Beck RE, Schultz JS (1970) Hindered diffusion in microporous membranes with known pore geometry. Science 170:1302–1305

Diecke FP, Ma L, Iserovich P, Fischbarg J (2007) Corneal endothelium transports fluid in the absence of net solute transport. Biochim Biophys Acta 1768:2043–2048

Donn A, Miller SL, Mallett NM (1963) Water permeability of the living cornea. Arch Ophthalmol 70:515–521

Durbin RP (1960) Osmotic flow of water across permeable cellulose membranes. J Gen Physiol 44:315–326

Echevarria M, Kuang K, Iserovich P, Li J, Preston GM, Agre P, Fischbarg J (1993) Cultured bovine corneal endothelial cells express CHIP28 water channels. Am J Physiol Cell Physiol 265:C1349–C1355

Fischbarg J (2010) Fluid transport across leaky epithelia: central role of the tight junction, and supporting role of aquaporins. Physiol Rev 90:1271–1290

Fischbarg J, Diecke FP (2005) A mathematical model of electrolyte and fluid transport across corneal endothelium. J Membr Biol 203:41–56

Fischbarg J, Warshavsky CR, Lim JJ (1977) Pathways for hydraulically and osmotically-induced water flows across epithelia. Nature 266:71–74

Fischbarg J, Diecke FP, Iserovich P, Rubashkin A (2006) The role of the tight junction in paracellular fluid transport across corneal

endothelium. Electro-osmosis as a driving force. J Membr Biol 210:117–130
Geroski DH, Hadley A (1992) Characterization of corneal endothelium cell cultured on microporous membrane filters. Curr Eye Res 11:61–72
Gierer A, Wirtz K (1953) Molekulare Theorie der Mikroreibun g. Z Naturforschung [C] 8a:532
Green K, Green MA (1969) Permeability to water of rabbit corneal membranes. Am J Physiol 217:635–641
Guo P, Weinstein AM, Weinbaum S (2003) A dual-pathway ultrastructural model for the tight junction of rat proximal tubule epithelium. Am J Physiol Renal Physiol 285:F241–F257
Hirsch M, Renard G, Faure JP, Pouliquen Y (1976) Formation of intercellular spaces and junctions in regenerating rabbit corneal endothelium. Exp Eye Res 23:385–397
Hodson SA, Lawton DM (1987) The apparent reflexion coefficient of the leaky corneal endothelium to sodium chloride is about one in the rabbit. J Physiol 385:97–106
Hodson S, O'Leary D, Watkins S (1991) The measurement of ox corneal swelling pressure by osmometry. J Physiol 434:399–408
Kim JH, Green K, Martinez M, Paton D (1971) Solute permeability of the corneal endothelium and Descemet's membrane. Exp Eye Res 12:231–238
Klyce SD, Russell SR (1979) Numerical solution of coupled transport equations applied to corneal hydration dynamics. J Physiol 292:107–134
Knipp GT, Ho NF, Barsuhn CL, Borchardt RT (1997) Paracellular diffusion in Caco-2 cell monolayers: effect of perturbation on the transport of hydrophilic compounds that vary in charge and size. J Pharm Sci 86:1105–1110
Lea EJ (1963) Permeation through long narrow pores. J Theor Biol 5:102–107
Lim JJ, Fischbarg J (1981) Electrical properties of rabbit corneal endothelium as determined from impedance measurements. Biophys J 36:677–695
Lim JJ, Liebovitch LS, Fischbarg J (1983) Ionic selectivity of the paracellular shunt path across rabbit corneal endothelium. J Membr Biol 73:95–102
Lohschmidt J (1995) On the size of the air molecules. J Chem Educ 72:870–875
Lyslo A, Kvernes S, Garlid K, Ratkje SK (1985) Ionic transport across corneal endothelium. Acta Ophthalmol 63:116–125
Ma L, Kuang K, Smith RW, Rittenband D, Iserovich P, Diecke FP, Fischbarg J (2007) Modulation of tight junction properties relevant to fluid transport across rabbit corneal endothelium. Exp Eye Res 84:790–798
Mishima S, Hedbys BO (1967) The permeability of the corneal epithelium and endothelium to water. Exp Eye Res 6:10–32
Mishima S, Trenberth SM (1968) Permeability of the corneal endothelium to nonoelectrolytes. Invest Ophthalmol Vis Sci 7:34–43
Narula PM, Xu M, Kuang K, Akiyama R, Fischbarg J (1992) Fluid transport across cultured bovine corneal endothelial cell monolayers. Am J Physiol Cell Physiol 262:C98–C103
Olsen T, Sperling S (1987) The swelling pressure of the human corneal stroma as determined by a new method. Exp Eye Res 44:481–490
Preisig PA, Berry CA (1985) Evidence for transcellular osmotic water flow in rat proximal tubules. Am J Physiol Renal Physiol 249:F124–F131
Rector FC, Berry CA (1982) Role of the paracellular pathway in reabsorption of solutes and water by proximal convoluted tubule of the mammalian kidney. In: Bradley SE, Purcell EF (eds) The paracellular pathway. Josiah Macy Jr. Foundation, New York, pp 135–158
Renkin EM (1954) Filtration, diffusion, and molecular sieving through porous cellulose membranes. J Gen Physiol 38:225–243
Reuss L (2008) Mechanisms of water transport across cell membranes and epithelia. In: Alpern RJ, Hebert SC (eds) Seldin and Giebisch's the kidney: physiology and pathophysiology. Elsevier Academic Press, Burlington, pp 147–168
Rubashkin A, Iserovich P, Hernandez J, Fischbarg J (2005) Epithelial fluid transport: protruding macromolecules and space charges can bring about electro-osmotic coupling at the tight junctions. J Membr Biol 208:251–263
Sanchez JM, Li Y, Rubashkin A, Iserovich P, Wen Q, Ruberti JW, Smith RW, Rittenband D, Kuang K, Diecke FPJ, Fischbarg J (2002) Evidence for a central role for electro-osmosis in fluid transport by corneal endothelium. J Membr Biol 187:37–50
Schafer JA, Andreoli TE (1986) Principles of water and nonelectrolyte transport across membranes. In: Andreoli TE, Hoffman JF, Fanestil DD, Schultz SG (eds) Physiology of membrane disorders. Plenum Medical Book, New York, pp 177–190
Shachar-Hill B, Hill AE (2002) Paracellular fluid transport by epithelia. Int Rev Cytol 215:319–350
Sobottka Ventura AC, Wälti R, Böhnke M (2001) Corneal thickness and endothelial density before and after cataract surgery. Br J Ophthalmol 85:18–20
Sun XC, Allen KT, Xie Q, Stamer WD, Bonanno JA (2001) Effect of AQP1 expression level on CO_2 permeability in bovine corneal endothelium. Invest Ophthalmol Vis Sci 42:417–423
Thau G, Bloch R, Kedem O (1966) Water transport in porous and non-porous membranes. Desalination 1:129–138
Van Itallie CM, Anderson JM (2004) The molecular physiology of tight junction pores. Physiology 19:331–338
Van Itallie CM, Anderson JM (2006) Claudins and epithelial paracellular transport. Annu Rev Physiol 68:403–429
Zhu F, Tajkhorshid E, Schulten K (2004) Theory and simulation of water permeation in aquaporin-1. Biophys J 86:50–57